RESEARCH ARTICLE | DECEMBER 11 2023

Water entry of spheres with impact-axis channels FREE

Md Emazuddin Alif [0]; Azeem Husain; Christopher Quizhpe [0]; Elias Maynor [0]; Andrew K. Dickerson 🗷 [0]

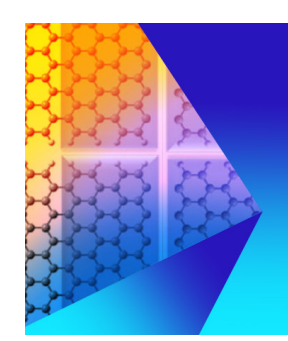


Physics of Fluids 35, 122109 (2023) https://doi.org/10.1063/5.0175406





CrossMark



Physics of Fluids Journal of Applied Physics

Special Topic: Recent Advances in Fluid Mechanics and Nanoelectronics: Memorializing ICRAFMN-2023

Submit Today!





Water entry of spheres with impact-axis channels

Cite as: Phys. Fluids **35**, 122109 (2023); doi: 10.1063/5.0175406 Submitted: 6 September 2023 · Accepted: 17 November 2023 ·







Published Online: 11 December 2023

Md Emazuddin Alif, 🕞 Azeem Husain, Christopher Quizhpe, 🕞 Elias Maynor, 🕞 and Andrew K. Dickerson 🗈 🕞

AFFILIATIONS

Mechanical, Aerospace, and Biomedical Engineering, University of Tennessee, Knoxville, Tennessee 37996, USA

a) Author to whom correspondence should be addressed: ad@utk.edu

ABSTRACT

Spheres are the most studied water entry projectile due to their symmetry and simplicity, but in practical applications, it is rare that an impacting body is perfectly spherical. Perturbations to the classical impactor are thus critical for aligning fundamental investigation with more advanced engineering applications. This study investigates the water entry of hydrophilic and hydrophobic spheres with through-channels along the water entry axis and producing deep seal cavities. The channels allow water to pass through the sphere to create a jet tailing the sphere and hastening cavity pinch-off. Channeled spheres produce smaller cavities than their intact counterparts and suppress the onset of cavity formation. Spheres with channels show similar drag coefficients as solid, intact spheres.

Published under an exclusive license by AIP Publishing. https://doi.org/10.1063/5.0175406

I. INTRODUCTION

At sufficient velocity, bodies entering water create air-entraining cavities that trail the impactor, reducing hydrodynamic drag, and a crown-like splash above. ¹⁻⁴ The appearance of these ubiquitous splash features are nearly independent of impactor shape. The physics behind such a familiar process and the scope of its application have beguiled fluid dynamicists and inspired a vast body of research. ^{3,5-16} A substantial amount of such work has involved modifications on the dynamics^{8,9,17-19} and surface properties ²⁰⁻²⁴ of the entering body. Here, we introduce a modification to the canonical water entry sphere, the introduction of an impact axis channel, and thereby add yet another complexity to the splash features of impacting spheres. A flow channel through our impactors permits the creation of free jets that trail the impactor, protruding above the free surface and undergoing Rayleigh breakup, as shown in Fig. 1.

The investigation of spherical impactors has been undertaken by a compendium of studies that have focused on cavity dynamics, $^{16,18,25-31}$ drag forces, 7,32 the influences of wettability, $^{5,21,33-37}$ alterations to the free surface, $^{22-24,38}$ and the entry dynamics of the spheres. $^{8,9,17-19}$ Barring few exceptions, cavity and drag features depend on the advancing contact angle of the impactor θ , the Weber number $\mathrm{We}_D = \rho D u^2/\sigma$, and the Froude number $\mathrm{Fr} = u/\sqrt{gD}$, where u is the impact velocity, ρ and σ are the density and the surface tension of water respectively, g is acceleration due to gravity, and D is the diameter of the impactor. Duez et al. found a transition velocity $u_{\rm crit}$ as a function of θ above which smooth spheres form airentraining cavities. 5,6 Below an advancing contact angle of 90°, the transition to cavity-forming impacts is independent of wettability. For $\theta > 90^\circ$, the transition velocity is a strong function of wettability.

Modifications to the classical free-falling homogeneous sphere are not new. Entry dynamics and heterogeneous surface modifications alter cavity morphology and impactor trajectory. The addition of spin on the body at impact produces an asymmetric cavity with a persistent wedge of fluid emerging across the center of gravity. Spin induces lift that causes horizontal migration, introducing curvature in the trajectory of the impacting sphere. 17-19 Pinch-off time is roughly constant for spheres and independent of spin rate and buoyancy.9 However, highly buoyant spheres display a significant decrease in the pinchoff depth. Heterogeneous wetting properties across a sphere produce asymmetric cavities and lateral migration similar to spinning spheres.³³ In addition to altered trajectories, heterogeneous spheres produce cavities at entry velocities below u_{crit} prescribed by Duez et al.⁶ For example, a hydrophilic sphere with a hydrophobic cap triggers flow separation to generate air-entraining cavities. Hydrophilic spheres impacting fabric resting on a liquid pool likewise induce flow separation to produce cavities. The cavities produced through such impacts are relatively deep, with correspondingly high Worthington jets and pronounced splash crowns.²²⁻²⁴ Horizontal grooves on hydrophilic spheres assist in air-entrainment; increasing the number of grooves reduces the functional u_{crit} , while reducing drag.³⁹ The inverted Leiden frost effect induced by heated spheres entering into a liquid pool creates a functionally non-wetting surface, producing very smooth cavity

Studies of non-spherical impactors are comparatively less numerous but have uncovered the criticality of entry geometry to the resulting impact sequence. The nose shape of a slender body dictates whether the cavity will be sufficiently voluminous to engulf the entire

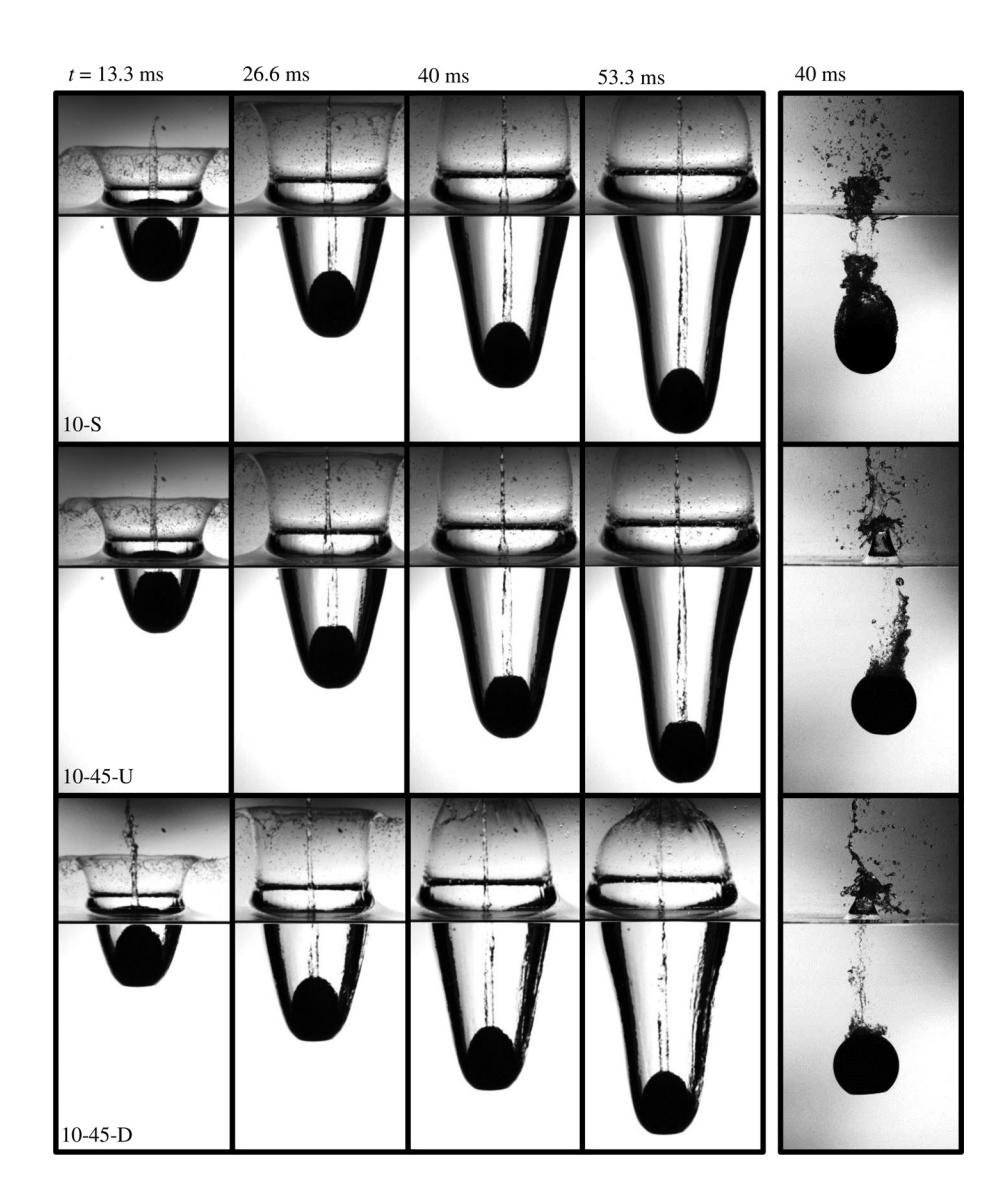


FIG. 1. Time sequences of impact for coated, superhydrophobic impactors with 10 mm channels at $u \approx 4.43$ m/s, Fr = 6.2. Channels are straight (top), with a tapered outlet (middle), and tapered inlet (bottom). The rightmost column corresponds to uncoated impactors of identical geometry along the same row. Multimedia available online.

impactor or if pinch-off will occur onto the projectile body. Short nonslender impactors may also experience cavity collapse onto the body as a result of a concave nose that stunts cavity development. Conical noses produce narrower, more slender cavities in comparison to spheres, whereas ogive noses produce larger and more open cavities. 1,40 Flat noses act similarly to disks, more prone to dome-over splashes than comparably sized slender bodies. Cupped or inverted ogive noses trap gas during impact, which leads to two divergent behaviors-cavity enhancement and suppression. Cavity growth or suppression can be modulated by controlling cup depth and impact conditions. 1,10 The sizes of such cavities are small but persist along the impacting body for longer as an evacuating gas torus surrounds the outer circumference.^{1,10} Flat noses and disks also trap air, although the trapped volume and entrapment timescale are decreased. 1,10 Radial symmetry of the impactor can also be perturbed to modulate cavity shape-Enriquez et al. produced a cavity shape similar to a pineapple

by using a radially symmetric 20-prong disk as the impacting body. 41,42

In this study, we employ radially symmetric, modified spheres with through-channels along their impact axis, as pictured in Fig. 1. We perform experiments at Fr = 4.1 and 6.2 with uncoated slightly hydrophobic ($\theta=107^\circ$) and coated superhydrophobic ($\theta>150^\circ$) impactors. We vary channel diameter and find the velocity at which uncoated impactors produce air-entraining deep seal cavities. We explore how these through-channels and the jets they produce influence cavity dynamics and hydrodynamic drag. We place our results in the context of greater water entry literature and discuss possible avenues of future work with spheres with interior passages.

II. METHODS

We manufacture our impactors by drilling through-holes (channels) into smooth phenolic resin spheres of mass $m = 131.1 \pm 0.9$ g

and diameter $D=52.5\,\mathrm{mm}$. A tapered end of either 45° or 60° is added to one end of the channels of select impactors with a lathe. We assign impactors a code "XX-YY-Z" where the placeholder "XX" represents the channel diameter in millimeters and "YY" is the taper angle in degrees, as schematized in Fig. 2(a). The final character "Z" in the impactor code represents the orientation of the taper at impact. "U" corresponds to the taper facing upward and "D" to the taper facing the water free surface. "S" indicates the impactor has no tapered hole and "C" impactors are intact spheres without holes. For example, the impactor "15–45-D" has a 15-mm through-hole, with a 45° tapered inlet as it enters the water. The unmodified exterior of our impactors has an advancing contact angle $\theta_a=107.6^\circ\pm2.3^\circ$. We increase the hydrophobicity of our impactors with a NeverWetTM coating to an advancing contact angle $\theta_a\geq150^\circ$. We clean and re-coat impactors after three trials.

Impactors are released from heights h = 0.43 and 1 m via a 3Dprinted guide that inserts into impactor channels, as schematized in Fig. 2(b). A unique guide is used for each channel size, ensuring impactors land with channels parallel to gravity. Our tank internally measures $24 \times 36 \times 48''$ (61 × 91 × 122 cm). Our tank size ensures wall effects are negligible⁴³-wall effects manifest as ripples on cavity walls which are not evidenced at the Froude numbers we employ. The impactor diameter (52.5 mm) is used as a visual scale to calibrate the digital imagery. The impacts are recorded at 3000 fps with a Photron Nova S6 fitted with a Nikon Micro-NIKKOR 55 mm f/2.8 lens. Zoom levels permit resolutions ranging from 0.35 to 0.55 mm/pixel. Custom light emitting diode (LED) lights and a 55% white translucent acrylic sheet diffuse backlighting for repeatable binarization in MATLAB. We track impactor position and measure dynamic quantities within binarized videos using bespoke code. We produce at least three replicates of each experimental condition. We digitally trace the left and right edge of the cavity starting from the water surface to the bottom of the sphere. Assuming an axisymmetric cavity, we consider the width of the cavity in each row of pixels to be the diameter of a flat disk, one

pixel in height. The diameter and height in pixels are converted to physical units to quantify the volume of each disk. The total volume of the cavity is obtained by summing individual disk volumes. In select trials, we track the topmost position of the splash crown in 1-ms intervals post-impact for 10 ms. The vertical velocity of the crown is calculated via linear interpolation of the crown position data.

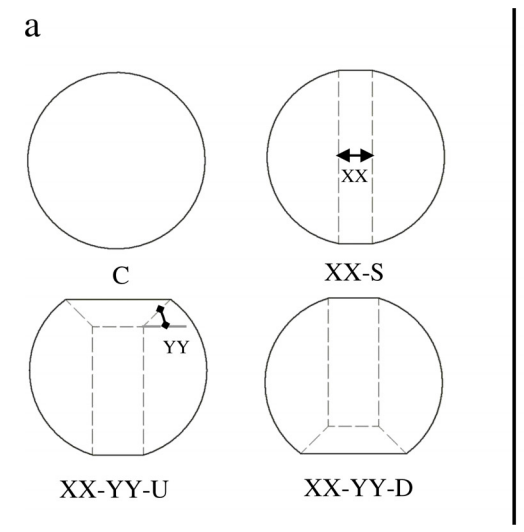
III. RESULTS

Two experimental release heights produce impact velocities corresponding to Froude numbers Fr=4.1 and 6.2. The most notable contrast of our impactors in this study from intact spheres, cylinders, and cups used in other studies is the emergence of a central jet formed by flow through the impactor. The central jet is observed for both cavity-forming impacts, Fig. 1 (left), and non-cavity-forming impacts, Fig. 1 (right). From image analysis we observe the presence of this jet hastens cavity pinch-off. We define pinch-off as occurring when the cavity necks to the jet diameter, thereby sealing the upper and lower air cavities from one another. The absence of a stagnation point at the leading pole of the impactor alongside a modified pinch-off time differentiates cavity volume and shape from those of intact control spheres (C). We discuss the various aspects of impact in turn.

A. Onset of cavity formation

The inclusion of a through-channel along the axis of impact eliminates the singular stagnation point at the front of a spherical impactor thereby modifying the flow around the sphere. It follows that such a modification will influence the transition from cavity-forming to non-cavity-forming impacts. Our experiments show that the presence of a channel coinciding with the impact axis suppresses the formation of cavities compared to intact spheres. The experimentally tuned, theoretical line for the transition to cavity formation of "C" spheres by Duez et al. 6 is given by the curve in Fig. 3(a).

Air-entraining cavities form behind spheres when the thin film moving along the circumference of the sphere has sufficient



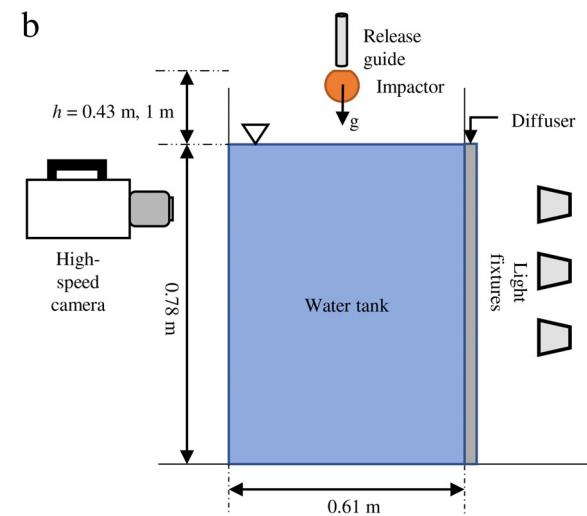


FIG. 2. (a) Cross-sectional diagrams of experimental impactors. "C" denotes the control sphere. "S" denotes straight channels without tapers. "U" and "D" denote up and down orientations of impactors with tapered channels, respectively. The placeholder "XX" denotes the channel diameter in mm (5, 10, 15). The placeholder "YY" denotes the angle of the taper in degrees (45, 60). (b) Schematic of the experimental setup.

momentum to separate, generating a three-phase contact line on the impactor surface. Selow the transition velocity, the liquid film adheres to the surface and no cavity is formed. The upward velocity of the film, ν is related to the impact velocity of the sphere u such that $u=\zeta\nu$, where ζ is a numerical prefactor on the order of unity [Fig. 4 (a)]. For a channeled impactor, a portion of the ascending film momentum is redirected through the channel, rather than along the periphery of the sphere, thereby reducing the magnitude of ζ [Fig. 4(b)]. The resulting reduction in film velocity is measurable if we assume that crown velocity and film velocity are directly correlated. For control spheres (C), we measure crown velocity to be 2.31 \pm 0.19 m/s (N=5) when impacting with Fr = 4.1. The 15-S impactor has a slower crown ascension at 2.27 \pm 0.10 m/s (N=4). The reduced film velocity permits greater entry velocities without flow separation. The transition velocities of 5-S, 10-S, and 15-S are 6% - 15% higher than

C spheres and 13% - 23% higher than that predicted by Duez *et al.* (2007), as shown in Fig. 3(a). The transition from non-cavity-forming to cavity-forming impacts for 15-S impactor is shown in time-stamped (*t*) photo sequences of Figs. 3(b) and 3(d).

The same three-phase dynamics that cause the formation of the splash crown ¹³ also occur inside the channel. The result is a jet that exits the impactor before the impactor passes the free surface, as shown in Fig. 1 (Multimedia View). The jet outpaces the crown skyward as shown in the left column of Fig. 1. We posit the confinement of the channel focuses the kinetic energy of the ascending film within the channel. At later times, flow inside the channel resembles undeveloped pipe flow and has a near-zero velocity relative to the lab frame as the sphere descends through the bath, evidenced by the apparent hovering of drops from broken jets in Fig. 1 (Multimedia View). In contrast, the Worthington jets following pinch-off are much faster than the nearly

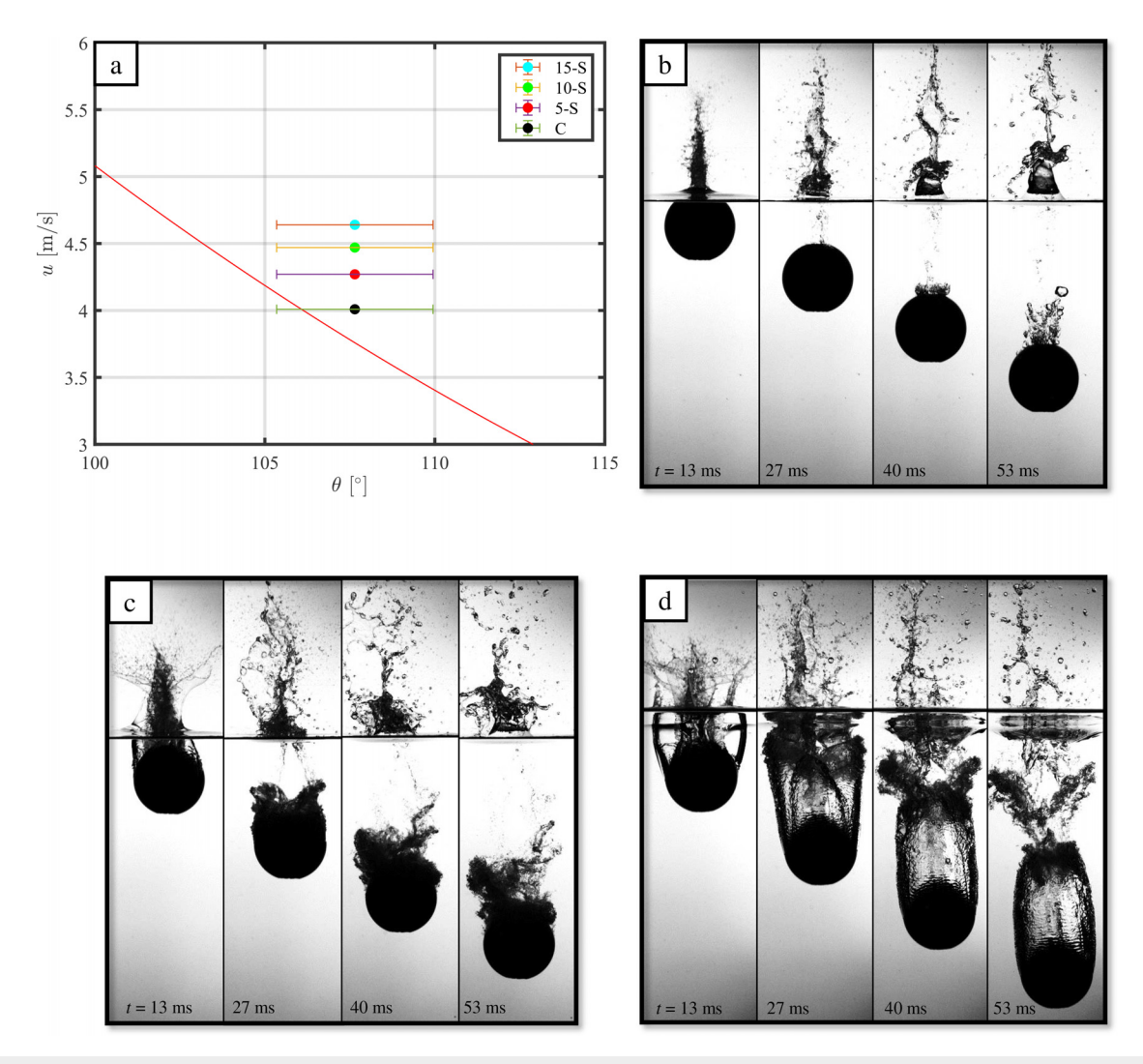


FIG. 3. Transition to cavity formation. (a) Cavity transition velocity u vs advancing contact angle θ . Channels in spheres suppress cavity formation. Image sequences of an uncoated, 15-S sphere impacting, (b) without cavity formation, u = 2.93 m/s, (c) at the transition to cavity formation, u = 4.64 m/s, and (d) with an air-entraining cavity, u = 6.00 m/s.

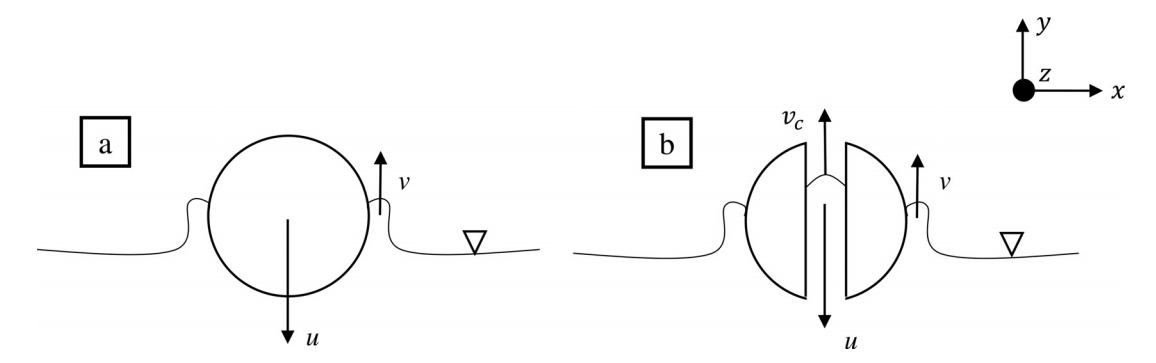


FIG. 4. Stability of the thin film adhering to the circumference of the impactor. (a) Thin films with sufficiently high v will separate from the impactor surface and form an entraining cavity. (b) Flow around a channeled impactor loses local momentum around the area of impact due to the flow inside the channel, v_c , and thus suppresses cavity formation.

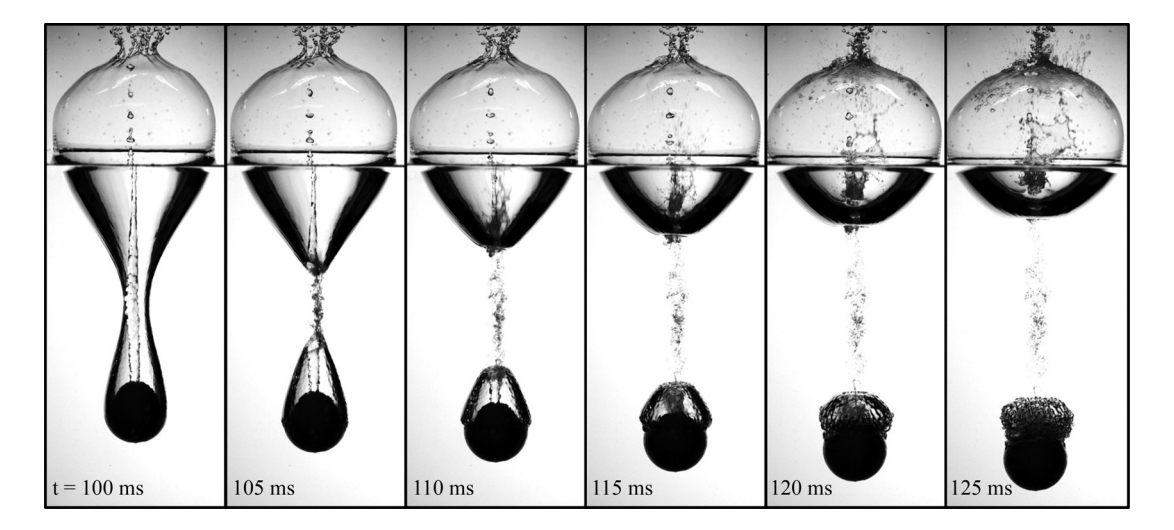


FIG. 5. Interactions between channel jet and Worthington jet for "10-S" impactor at Fr = 4.1. The Worthington jet fractures the channel jet by ascending with a much greater velocity.

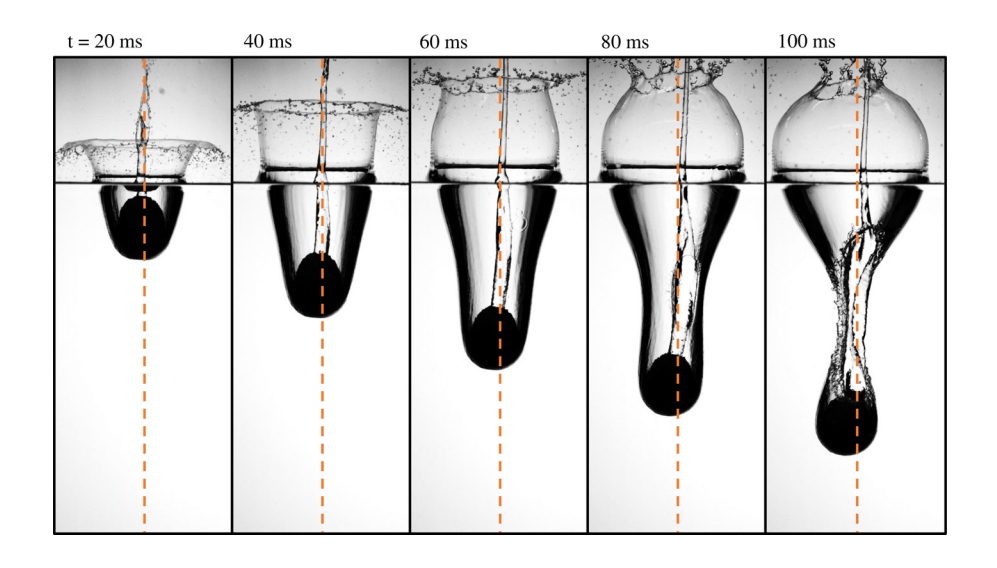


FIG. 6. Time sequences of off-axis impact for coated, superhydrophobic "15-60-D" impactors at $u\approx 2.93$ m/s, Fr =4.1. Off-axis impacts generate lateral migration. Multimedia available online.

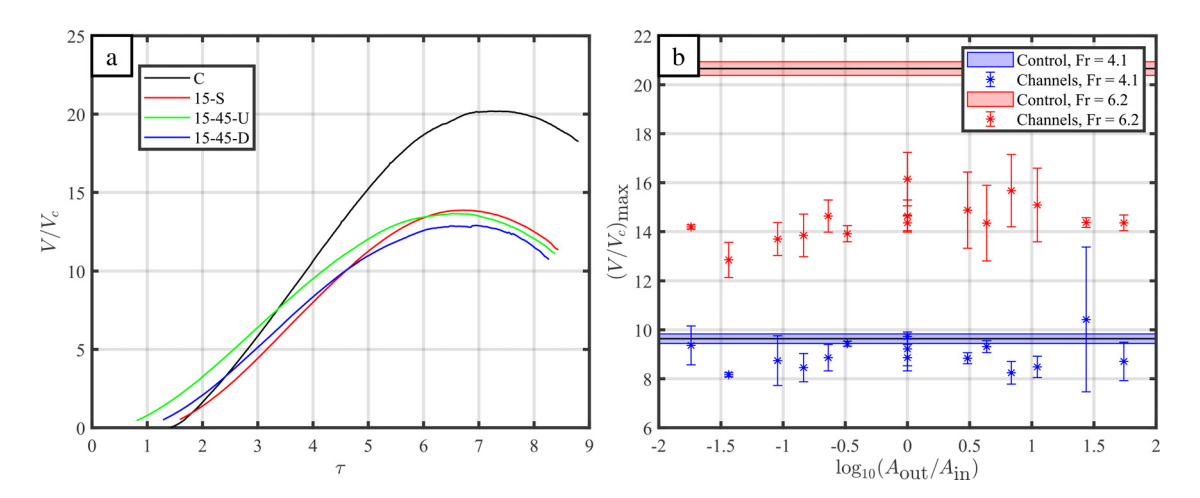


FIG. 7. (a) Normalized cavity volume, V/V_c vs τ . Fr = 6.2. Channeled spheres produce smaller cavities than their intact counterparts. (b) V/V_c vs logarithmic channel area ratio $\log_{10}(A_{out}/A_{in})$ at its maximum. Control spheres without channels are represented by horizontal shaded regions that denote their average V/V_c and standard deviation.

static channel jets. As a result, the interaction of the two jets is destructive. The Worthington jet slams into the channel jet with a much higher velocity, thereby fragmenting both jets in the interaction, as shown in Fig. 5.

B. Cavity dynamics

Superhydrophobic coated impactors striking the water free surface form air-entraining deep seal cavities for all test heights at all impact orientations. A deep seal cavity is observed when the first pinch-off occurs closer to the impactor, between one-third to one-half the distance from the impactor to the free surface. In contrast to canonical water entry studies, a central jet forms at the north pole of our impactors due to flow through their channels (Fig. 1). Off-axis

impacts, a result of misalignment between the channel and the falling path, result in through-impactor jets that collide with cavity walls, as shown in Fig. 6 (Multimedia View). Cavities that are impacted by jets are asymmetric and are accompanied by lateral migration of the impactor.³³ We exclude impacts that occur off-axis in our study.

The change in cavity volume V over dimensionless time $\tau = tu/D$ for different impactors starting from water entry to pinchoff is shown in Fig. 7(a). Cavity volume increases quasi-linearly with time for all impact orientations until $\tau \approx 5$, after which the rate of volume growth slows. Cavity volume begins decreasing at $\tau \approx 7$ until pinch-off at $\tau > 8$. The cavity volume of control impactors ("C") remains higher from $\tau \gtrsim 3.5$, especially at pinch-off. The normalized maximum cavity volume $(V/V_C)_{\rm max}$ vs the logarithmic area ratio of the outlet and the inlet of the impactor $\log_{10}(A_{\rm out}/A_{\rm in})$, where V_C is

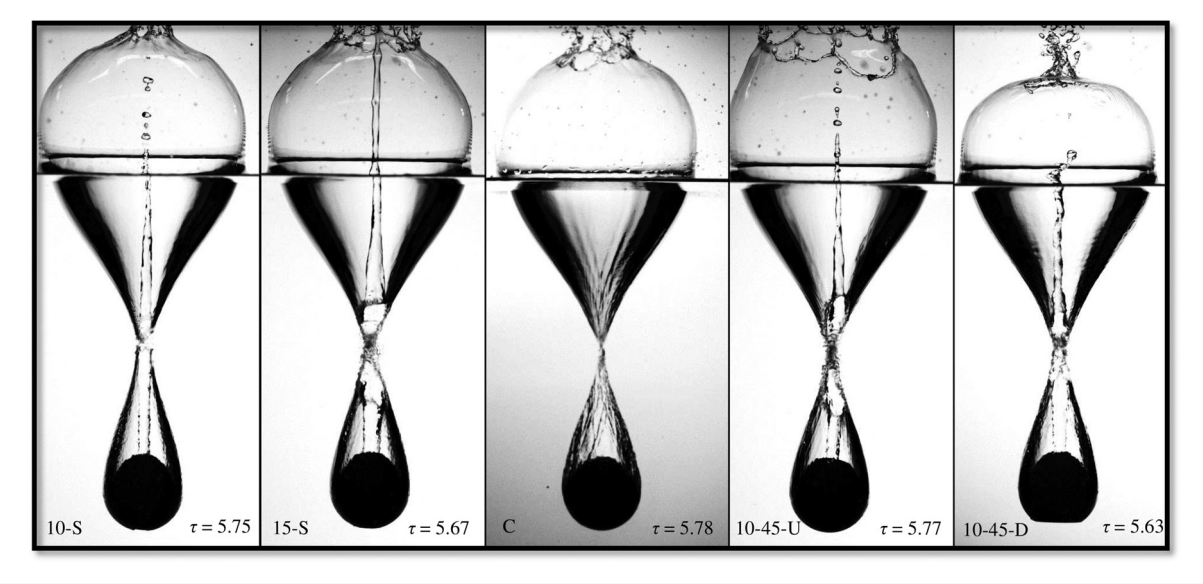


FIG. 8. The instant of pinch-off for "10-S," "15-S," "C," "10-45U," and "10-45D." Fr=4.1.

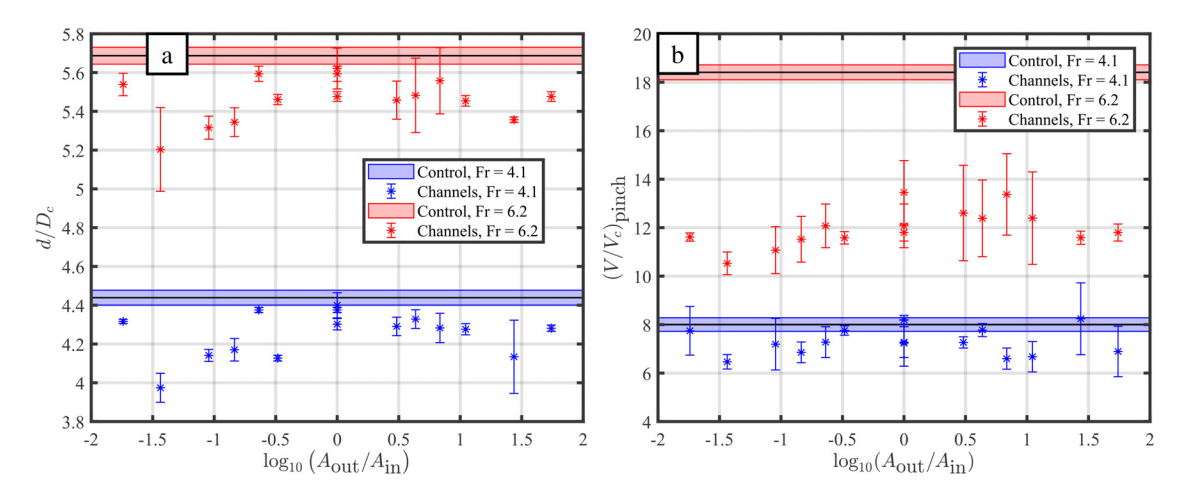


FIG. 9. (a) Normalized pinch-off depth d/D_c vs logarithmic channel area ratio $\log_{10}(A_{\text{out}}/A_{\text{in}})$. Jets emerging from cavities precipitate pinch-off, thus lowering pinch-off depth. The control spheres without channels are represented by horizontal shaded regions that denote their average d/D_c and standard deviation. (b) V/V_c vs $\log_{10}(A_{\text{out}}/A_{\text{in}})$ at pinch-off.

the volume of the control sphere, is shown in Fig. 7(b). A value of $\log_{10}(A_{\rm out}/A_{\rm in})=0$ corresponds to an "S" impactor, and positive and negative values imply "U" and "D" impactors, respectively. When compared to a control sphere ("C"), cavities from channeled impactors are lower in maximum volume across all Froude numbers. Liquid displacement during contact with the water surface determines the cavity volume of the impactors. As a "C" impactor contacts the water surface, the liquid is displaced radially outward at the stagnation point, resulting in the widest base a sphere can provide for cavity generation. For a channeled impactor, liquid displacement begins at the perimeter of the inlet, where the liquid is forced radially at a shallower angle to produce a more slender cavity. Such discrepancies between channel and control impactors are more pronounced as the Froude number Fr increases, as shown by the distance of data points from control lines in Fig. 7(b).

Pinch-off occurs at shorter τ for channeled impactors as shown in Fig. 7(a). The precipitation of pinch-off is a direct consequence of narrower cavities and trailing jet interaction with collapsing cavity

walls as pictured in Fig. 8. The result is a reduction in the pinch-off depth d as shown in Fig. 9(a). Unlike cavity volume, the disparity in pinch-off depth between channeled and intact impactors does not increase with the Froude number. The disproportionate change in cavity volume at higher Froude numbers, as shown in Fig. 9(b), reinforces our earlier assertion that control impactors produce wider cavities. "S" impactors demonstrate a pinch-off depth that is most similar to "C" impactors. "C" impactors are heaviest and thus carry the most kinetic energy at impact. However, we find no apparent relation between impactor mass and cavity volume as shown in Figs. 10(a) and 10(b). The discrepancy between channeled impactors and their control is again more pronounced at the higher of our two experimental Froude numbers, plotted in Fig. 10(b).

Channel outlet conditions have an effect on pinch-off depth and stability of the channel jet, as seen by comparing between "S" and "-60-U" trials for 5-mm and 10-mm impactors in Fig. 11. "U" impactors experience less drag and produce more stable channel jets.

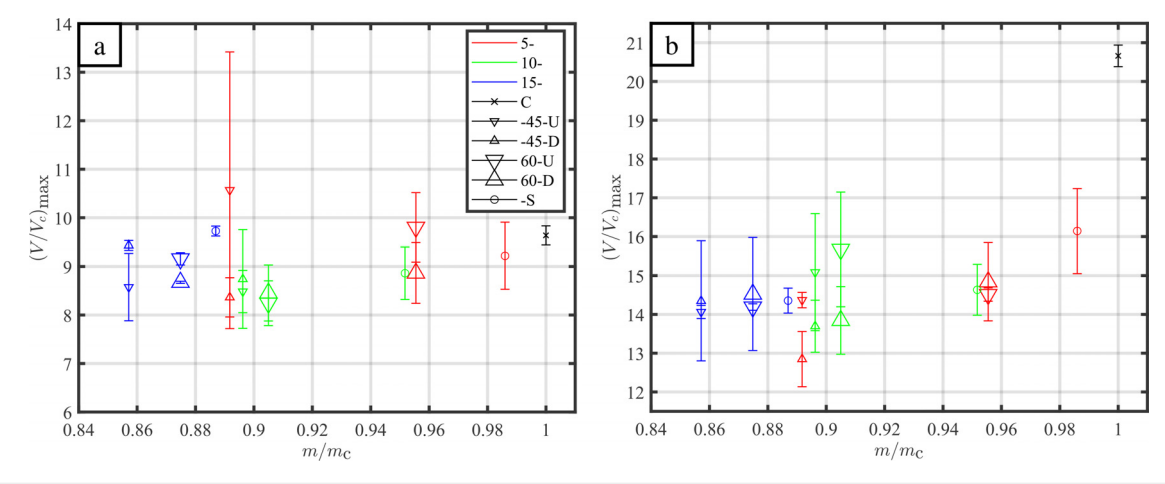
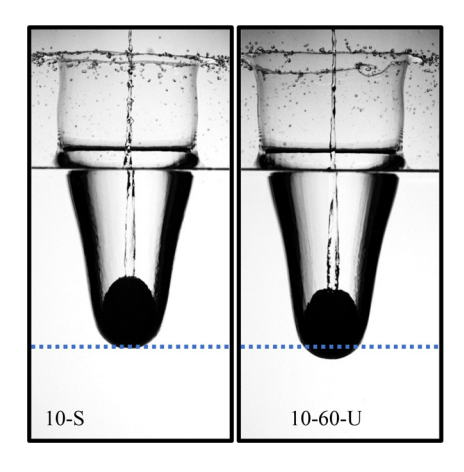


FIG. 10. V/V_c at maximum cavity volume vs mass ratio m/m_c for (a) Fr = 4.1 and (b) Fr = 6.2. We find no apparent relationship between impactor mass and cavity volume.



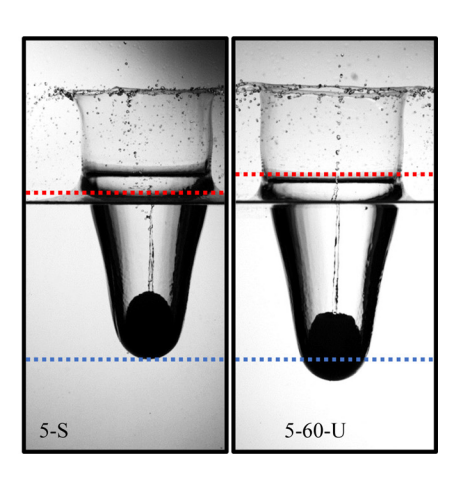


FIG. 11. "S" and "U" channels are not equivalent. Left and right image pairs compare "S" and "U" impacts for 10-mm and 5-mm channels at $\tau=4.2$. "U" impactors experience less drag and produce more stable jets. The blue lines denote the bottom of the "S" impactor. Red lines in the right pair denote the approximate breakup location of the jets. Jets in the left pair breakup out of frame.

The stability of the jet can be inferred from the longer breakup distance of "5-60-U" impactor compared to "5-8" impactor, and from reduced perturbations on the surface of the jet in "10-60-U" impactor in comparison to "10-8" impactor. Intuition suggests that the outlet conditions of "S" impactors produce more stable, or at least equivalently stable, jets compared to "U" impactors. However, the channel length in "S" impactors is between 32% and 82% longer than those of "U" impactors due to the absence of tapers. In traditional jetting systems, longer jet nozzles generally produce less stable jets, believed to be the result of increased turbulence from a longer passage. 44

C. Drag analysis

To compare the hydrodynamic forces experienced by different impactors in all orientations, we track the bottom of the impactors (Fr = 4.1, 6.2) from the free surface contact to pinch-off. The position data of the bottom of the impactors are fit to a smoothing spline 45 corresponding to a quintic polynomial, such that the initial and final jerk is zero. The acceleration experienced by the impactor is extracted by taking the second derivative of the smoothed data. We consider the positive y-axis pointing against the direction of motion (Fig. 4). Channeled impactors experience higher positive acceleration compared to their intact counterparts for all τ , as shown in Fig. 12(a). As shown previously, 1,27,46 larger cavities correspond to higher drag, so it is counter-intuitive that channeled impactors decelerate more aggressively than "C" spheres [Fig. 12(a)]. While the presence of an entryaxis channel removes the stagnation point, it introduces a stagnation circle. We believe the presence of such a circle along with the shear forces inside the channel compensate for the supposed lower drag that would be observed from narrow cavities. Time-averaged values of acceleration a_{avg} from free surface contact to pinch-off are plotted against $\log_{10}(A_{\text{out}}/A_{\text{in}})$ in Fig. 12(b). Non-intuitively, "D" impactors do not exhibit markedly greater positive accelerations than "U" impactors. The leftmost point at Fr = 6.2, corresponding to $\log_{10}(A_{\text{out}}/A_{\text{in}}) = -1.74$ experiences notably higher acceleration than other impactors. This 5-45-D impactor has relatively restricted flow in the channel, thereby acting the most like an impacting cup.

The salient forces acting on the entering impactors are gravity, buoyancy and drag, with a force balance described by

$$(m + m_a)\ddot{y} = \frac{1}{2}C_D\rho\pi D^2\dot{y}^2 + \frac{1}{2}\rho gV - mg,$$
 (1)

where $m_{\rm a} = \pi \rho D^3 C_{\rm m}/6$ is the added mass and $C_{\rm m}$ is the added mass coefficient. Solving Eq. (1) for the hydrodynamic drag coefficient

$$C_{\rm D} = \frac{2\left[(m + \pi \rho D^3 C_{\rm m}/6) \ddot{y} - \frac{1}{2} \rho g V + mg \right]}{\rho \pi D^2 \dot{y}^2}.$$
 (2)

The choice of $C_{\rm m}$ is not obvious, particularly when impactors have varying geometries. By setting $C_{\rm m}=0.25,0.5,0.75$, and 1, we find $C_{\rm D}$ varies up to 24% for "C" spheres. We select $C_{\rm m}=0.5$ for "C" impactors based on previous works. 3,8,9,17,19,23,33 Channeled spheres deflect water differently than an intact sphere (Sec. III B), such that when channel diameter $d_{\rm c} \rightarrow D, C_{\rm m} \rightarrow 0$, and for $d_{\rm c} \rightarrow 0$, $C_{\rm m} \rightarrow 0.5$. Therefore, for channeled impactors, we multiply an area correction factor to $C_{\rm m}$, such that $C_{\rm m}=0.5\times(D^2-d_{\rm c})/D^2$. For 5-,10- and 15-mm channels, $C_{\rm m}$ varies up to a modest 9% in comparison to that for "C" impactors. Our area correction factor thus demonstrates that our channels have only a slight effect on added mass. It is no surprise then that our drag model is insensitive to the value of $C_{\rm m}$ induced by the area correction factor, as seen in Figs. 12(c) and 12(d).

From our force balance in Eq. (2) we calculate temporal C_D values for our various impactors. Based on the temporal acceleration in Fig. 12(a) and insensitivity to C_m , one may expect C_D for channeled impactors to be markedly greater than "C" spheres. However, boring a channel through an impactor reduces its mass and buoyant force such that C_D values across all our impactors are nearly indistinguishable. Future development of the above drag model may include an internal shear force term for undeveloped channel flow and a more precise accounting of buoyant force.

IV. DISCUSSION

In this study, we explore how the inclusion of a through-channel in the classical water entry sphere modifies the onset of cavity formation, cavity volume and pinch-off, and hydrodynamic drag. Our study demonstrates that internal, rather than external, projectile features can be incorporated to alter the most salient characteristics in a water entry event. Channel permutations that future researchers and engineers may explore are abundant and may include those with bends, which will induce more intense lateral migration. The location of the off-axis jet exit provides passive control for lateral movement. The lateral migration caused by the off-axis orientation of the channels in our impactors is relatively slight, less than that witnessed for spheres

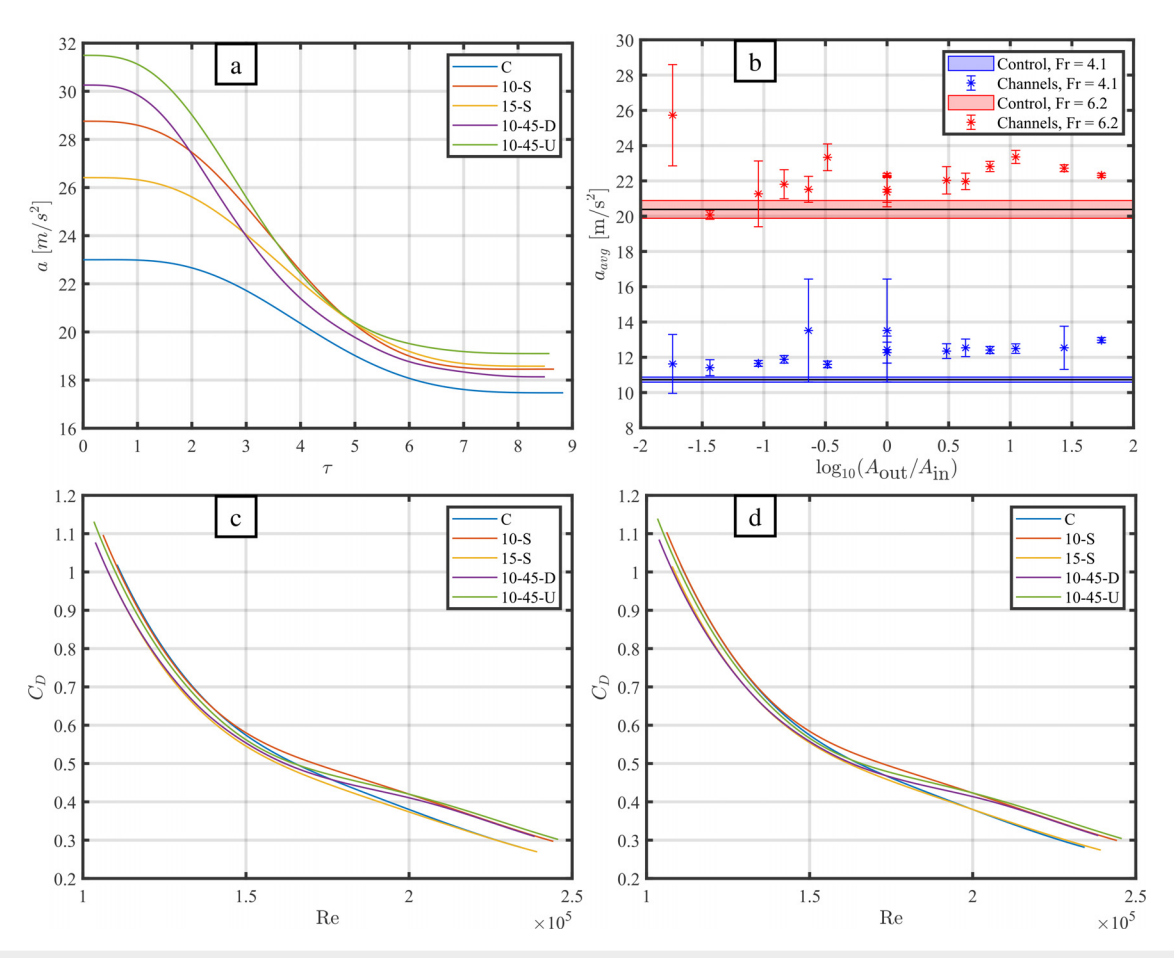


FIG. 12. Hydrodynamic drag. (a) Acceleration of "C," "10-S," "10-45U," "10-45D," a vs τ . (b) Average acceleration, a_{avg} vs logarithmic channel area ratio $\log_{10}(A_{out}/A_{in})$. (c) Drag co-efficient, C_D vs Re for geometry-dependent added mass coefficient C_m . (d) C_D vs Re for constant $C_m = 0.5$.

entering with spin^{17–19} and those heterogeneously coated hydrophobic.³³ If our impactors are intentionally released off-axis, lateral migration is aggressive and comparable to other methods.

The control of inlet and outlet geometries can be exploited to have greater control over cavity dynamics. Channels with carefully flared, hydrophilic outlets can, through adhesion to the channel wall, break the exiting jet into a radial spray that impacts cavity walls and induces greater drag. The behavior of such through-channel jets that attempt to exploit adhesion will, of course, be highly dependent on entry velocity. With smaller channels than those tested or with internal flow restrictions, channels will behave as functionally closed or induce cavitation. Inducing cavitation inside the channel may have significant consequences on entry and jet dynamics. We expect closed or functionally closed channels to behave much like the impact of cups studied recently, such that gas entrapment and release from the cup is dependent on cup geometry and impact speed. ¹⁰

The entry of projectiles into non-Newtonian fluids has received some attention 47-51 but remains largely unexplored. An untested method for modulating drag and cavity morphology of channeled impactors is the usage of non-Newtonian fluids as the liquid bath. The impact of channeled spheres in non-Newtonian fluids will have a

diametric effect on the drag properties compared to Newtonian fluids. We believe the shear stress inside the channel is compensating for the removal of the stagnation point due to the presence of the channel. A non-Newtonian fluid bath will result in under- and over-compensation, depending on the rheological properties of the liquid.

V. CONCLUSION

In this study, we examine the free surface impact of 52.5-mm diameter spheres into water for Fr=4.1 and 6.2. Spheres have been modified to include a circular channel along the axis of impact, with diameters 5, 10, and 15 mm. The channels have two broad configurations, straight and tapered inlet-outlet geometry, such that one end has a greater diameter than the through-channel. The allowance of passage through the impactor eliminates the stagnation point on the leading surface and introduces a stagnation ring. The result is a suppression of air-entraining cavity formation that would otherwise be experienced by a solid sphere. Larger diameter channels express greater cavity suppression. Liquid passage through the channel results in a free jet trailing the sphere, the presence of which precipitates cavity pinch-off. A more rapid pinch-off decreases the depth at which pinch-off occurs in relation to that experienced by a solid sphere. The presence of a

channel in the impact axis reduces the maximum cavity volume and cavity volume at pinch-off; intact spheres produce the greatest maximum cavity volume. Despite the alterations channels produce in the localized flow field around the sphere, channels and their configurations do not notably augment the drag coefficient at entry. A hydrodynamic force model remains insensitive to added mass coefficients as reported previously with solid spheres.

VI. DATA ACCESS

Raw experimental videos and data are publicly available in perpetuity via OneDrive. Interested parties should contact the corresponding author for access.

ACKNOWLEDGMENTS

We would like to thank the National Science Foundation (CBET-1941341) for support, Tadd T. Truscott for fruitful discussions, and V. Chakpuang, J. Saengsawang, F. Mohsun, and R. Syed for experimental contributions.

AUTHOR DECLARATIONS Conflict of Interest

The authors have no conflicts to disclose.

Author Contributions

Md Emazuddin Alif: Conceptualization (supporting); Data curation (lead); Formal analysis (lead); Investigation (lead); Methodology (equal); Supervision (supporting); Validation (equal); Visualization (lead); Writing – original draft (lead); Writing – review & editing (equal). Azeem Husain: Data curation (supporting); Formal analysis (supporting); Investigation (supporting); Methodology (supporting). Christopher Quizhpe: Data curation (supporting); Formal analysis (supporting); Investigation (supporting); Methodology (supporting). Elias Maynor: Data curation (supporting); Formal analysis (supporting); Investigation (supporting); Methodology (supporting). Andrew Keith Dickerson: Conceptualization (lead); Formal analysis (supporting); Funding acquisition (lead); Investigation (supporting); Methodology (lead); Project administration (lead); Resources (lead); Supervision (lead); Visualization (supporting); Writing – original draft (equal); Writing – review & editing (equal).

DATA AVAILABILITY

The data that support the findings of this study are available from the corresponding author upon reasonable request.

REFERENCES

- ¹T. T. Truscott, B. P. Epps, and J. Belden, "Water Entry of Projectiles," Annu. Rev. Fluid Mech. **46**, 355–378 (2014).
- ²D. Gilbarg and R. A. Anderson, "Influence of atmospheric pressure on the phenomena accompanying the entry of spheres into water," J. Appl. Phys. 19, 127–139 (1948).
- ³J. M. Aristoff and J. W. M. Bush, "Water entry of small hydrophobic spheres," J. Fluid Mech. **619**, 45–78 (2009).
- ⁴J. Eshraghi, S. Jung, and P. P. Vlachos, "To seal or not to seal: The closure dynamics of a splash curtain," Phys. Rev. Fluids 5, 104001 (2020).
- 5C. Duez, C. Ybert, C. Clanet, and L. Bocquet, "Wetting controls separation of inertial flows from solid surfaces," Phys. Rev. Lett. 104, 084503 (2010).

- ⁶C. Duez, C. Ybert, C. Clanet, and L. Bocquet, "Making a splash with water repellency," Nat. Phys. 3, 180–183 (2007).
- ⁷A. May and J. C. Woodhull, "The virtual mass of a sphere entering water vertically," J. Appl. Phys. 21, 1285–1289 (2004).
- ⁸J. M. Aristoff, T. T. Truscott, A. H. Techet, and J. W. M. Bush, "The water-entry cavity formed by low Bond number impacts," Phys. Fluids 20, 091111 (2008).
- ⁹J. M. Aristoff, T. T. Truscott, A. H. Techet, and J. W. M. Bush, "The water entry of decelerating spheres," Phys. Fluids **22**, 032102 (2010).
- ¹⁰J. Belden, N. B. Speirs, A. M. Hellum, M. Jones, A. J. Paolero, and T. T. Truscott, "Water entry of cups and disks," J. Fluid Mech. 963, A14 (2023).
- ¹¹Y. Hou, Z. Huang, Z. Chen, Z. Guo, and Y. Luo, "Investigations on the vertical water-entry of a hollow cylinder with deep-closure pattern," Ocean Eng. 190, 106426 (2019).
- ¹²R. C. Hurd, J. Belden, M. A. Jandron, D. Tate Fanning, A. F. Bower, and T. T. Truscott, "Water entry of deformable spheres," J. Fluid Mech. **824**, 912–930 (2017)
- ¹³A. A. Korobkin and V. V. Pukhnachov, "Initial stage of water impact," Annu. Rev. Fluid Mech. 20, 159–185 (1988).
- ¹⁴N. B. Speirs, J. Belden, Z. Pan, S. Holekamp, G. Badlissi, M. Jones, and T. T. Truscott, "The water entry of a sphere in a jet," J. Fluid Mech. 863, 956–968 (2019).
- 15H. Liu, J. Pi, B. Zhou, L. Chen, Q. Fu, and G. Zhang, "Experimental investigation on the multiphase flow characteristics of oblique water entry of semi-closed cylinder," Ocean Eng. 239, 109819 (2021).
- ¹⁶L. Yang, Y. Wei, J. Li, C. Wang, and W. Xia, "Experimental study on splash behaviors and cavity shape of elastic spheres during water entry," Appl. Ocean Res. 113, 102754 (2021).
- ¹⁷T. T. Truscott and A. H. Techet, "Water entry of spinning spheres," J. Fluid Mech. 625, 135–165 (2009).
- 18 T. T. Truscott and A. H. Techet, "Cavity formation in the wake of a spinning sphere impacting the free surface." Phys. Fluids 18, 091113 (2006)
- sphere impacting the free surface," Phys. Fluids 18, 091113 (2006).

 19 A. Techet and T. Truscott, "Water entry of spinning hydrophobic and hydrophilic spheres" J. Fluids Struct 27, 716–776 (2011)
- philic spheres," J. Fluids Struct. 27, 716–726 (2011).

 A. May, "Effect of surface condition of a sphere on its water-entry cavity,"
 J. Appl. Phys. 22, 1219–1222 (1951).
- ²¹N. B. Speirs, M. M. Mansoor, J. Belden, and T. T. Truscott, "Water entry of spheres with various contact angles," J. Fluid Mech. 862, R3 (2019).
- ²²D. A. Watson, C. J. Souchik, M. P. Weinberg, J. M. Bom, and A. K. Dickerson, "Making a splash with fabrics in hydrophilic sphere entry," J. Fluids Struct. 94, 102907 (2020)
- ²³D. A. Watson, J. L. Stephen, and A. K. Dickerson, "Jet amplification and cavity formation induced by penetrable fabrics in hydrophilic sphere entry," Phys. Fluids 30, 082109 (2018).
- ²⁴D. A. Watson, J. L. Stephen, and A. K. Dickerson, "Impacts of free-falling spheres on a deep liquid pool with altered fluid and impactor surface conditions," JoVE 144, e59300 (2019).
- ²⁵N. B. Speirs, Z. Pan, J. Belden, and T. T. Truscott, "The water entry of multi-droplet streams and jets," J. Fluid Mech. 844, 1084 (2018).
- ²⁶M. Lee, R. G. Longoria, and D. E. Wilson, "Cavity dynamics in high-speed water entry," Phys. Fluids 9, 540–550 (1997).
- ²⁷T. T. Truscott, "Cavity dynamics of water entry for spheres and ballistic projectiles," thesis, Massachusetts Institute of Technology, 2009.
- ²⁸J.-F. Louf, B. Chang, J. Eshraghi, A. Mituniewicz, P. P. Vlachos, and S. Jung, "Cavity ripple dynamics after pinch-off," J. Fluid Mech. 850, 611-623 (2018).
- ²⁹T. Grumstrup, J. B. Keller, and A. Belmonte, "Cavity ripples observed during the impact of solid objects into liquids," Phys. Rev. Lett. 99, 114502–114502 (2007).
- ³⁰A. Kiyama, M. M. Mansoor, N. B. Speirs, Y. Tagawa, and T. T. Truscott, "Gelatine cavity dynamics of high-speed sphere impact," J. Fluid Mech. 880, 707–722 (2019).
- ³¹M. M. Mansoor, I. U. Vakarelski, J. O. Marston, T. T. Truscott, and S. T. Thoroddsen, "Stable-streamlined and helical cavities following the impact of Leidenfrost spheres," J. Fluid Mech. 823, 716–754 (2017).
- ³²A. May and J. C. Woodhull, "Drag coefficients of steel spheres entering water vertically," J. Appl. Phys. 19, 1109–1121 (2004).

- ³³D. A. Watson, J. M. Bom, M. P. Weinberg, C. J. Souchik, and A. K. Dickerson, "Water entry dynamics of spheres with heterogeneous wetting properties," Phys. Rev. Fluids 6, 044003 (2021).
- ³⁴E. Dussan, "On the ability of drops or bubbles to stick to non-horizontal surfaces of solids. Part 2. Small drops or bubbles having contact angles of arbitrary size," J. Fluid Mech. 151, 1 (1985).
- 35 J. H. Snoeijer and B. Andreotti, "Moving contact lines: Scales, regimes, and dynamical transitions," Annu. Rev. Fluid Mech. 45, 269–292 (2013).
- ³⁶J. O. Marston, I. U. Vakarelski, and S. T. Thoroddsen, "Cavity formation by the impact of Leidenfrost spheres," J. Fluid Mech. **699**, 465–488 (2012).
- 37J. O. Marston, T. T. Truscott, N. B. Speirs, M. M. Mansoor, and S. T. Thoroddsen, "Crown sealing and buckling instability during water entry of spheres," J. Fluid Mech. 794, 506–529 (2016).
- ³⁸N. B. Speirs, M. M. Mansoor, R. C. Hurd, S. I. Sharker, W. G. Robinson, B. J. Williams, and T. T. Truscott, "Entry of a sphere into a water-surfactant mixture and the effect of a bubble layer," Phys. Rev. Fluids 3, 104004 (2018).
- 39 A. Mehri and P. Akbarzadeh, "Water entry of grooved spheres: Effect of the number of grooves and impact velocity," J. Fluids Struct. 100, 103198 (2021).
- ⁴⁰J. O. Marston and S. T. Thoroddsen, "Ejecta evolution during cone impact," J. Fluid Mech. 752, 410–438 (2014).
- ⁴¹O. R. Enriquez, I. R. Peters, S. Gekle, L. E. Schmidt, D. Lohse, and D. van der Meer, "Collapse and pinch-off of a non-axisymmetric impact-created air cavity in water," J. Fluid Mech. 701, 40–58 (2012).

- ⁴²O. R. Enríquez, I. R. Peters, S. Gekle, L. E. Schmidt, D. van der Meer, and D. Lohse, "Non-axisymmetric impact creates pineapple-shaped cavity," Phys. Fluids 23, 091106 (2011).
- ⁴³M. M. Mansoor, J. O. Marston, I. U. Vakarelski, and S. T. Thoroddsen, "Water entry without surface seal: Extended cavity formation," J. Fluid Mech. 743, 295–326 (2014).
- ⁴⁴A. Osta and K. A. Sallam, "Effect of Nozzle Length/Diameter ratio on the breakup of liquid jets in crossflow," AIAA Paper No. 2008-1040, 2008.
- ⁴⁵B. P. Epps, T. T. Truscott, and A. H. Techet, "Evaluating derivatives of experimental data using smoothing splines," *Proceedings of Mathematical Methods in Engineering International Symposium* (MMEI, Lisbon Portugal, 2010), pp. 29–38.
- ⁴⁶K. G. Bodily, S. J. Carlson, and T. T. Truscott, "The water entry of slender axisymmetric bodies," Phys. Fluids 26, 072108 (2014).
- ⁴⁷B. Akers and A. Belmonte, "Impact dynamics of a solid sphere falling into a viscoelastic micellar fluid," J. Non-Newtonian Fluid Mech. 135, 97–108 (2006).
- ⁴⁸J. M. Cheny and K. Walters, "Extravagant viscoelastic effects in the Worthington jet experiment," J. Non-Newtonian Fluid Mech. 67, 125–135 (1996).
- 49 T. C. de Goede, K. G. de Bruin, and D. Bonn, "High-velocity impact of solid objects on Non-Newtonian Fluids," Sci. Rep. 9, 1250 (2019).
- 50S. Nigen and K. Walters, "On the two-dimensional splashing experiment for Newtonian and slightly elastic liquids," J. Non-Newtonian Fluid Mech. 97, 233-250 (2001).
- ⁵¹H. Tabuteau, D. Sikorski, S. J. de Vet, and J. R. de Bruyn, "Impact of spherical projectiles into a viscoplastic fluid," Phys. Rev. E 84, 031403 (2011).